Journal of AppliedMath 2024, 2(2), 451.
https://doi.org/10.59400/jam.v2i2.451

Article

H∞ hybrid control and MRD in a steel frame building subjected to excessive vibrations caused by the dynamic action of wind and earthquake

Michael Dowglas de Gois Silva[1,*], Fábio Roberto Chavarette[2]

[1] Department of Mechanical Engineering, Faculty of Engineering of Ilha Solteira, UNESP-Paulista State University, Ilha Solteira, São Paulo 15385-000, Brasil
[2] Department of Engineering, Physics and Mathematics, Institute of Chemistry, UNESP-Paulista State Univerity, Araraquara, São Paulo 14800-060, Brasil
*** Corresponding author:** Michael Dowglas de Gois Silva, michael.dowglas@unesp.br

CITATION

de Gois Silva MD, Chavarette FR. H∞ hybrid control and MRD in a steel frame building subjected to excessive vibrations caused by the dynamic action of wind and earthquake. Journal of AppliedMath. 2024; 2(2): 451. https://doi.org/10.59400/jam.v2i2.451

ARTICLE INFO

Received: 4 January 2024
Accepted: 6 February 2024
Available online: 2 April 2024

Abstract: The dynamic loads from earthquakes and winds can destroy lives, cause collapse in civil structures, and interrupt basic services provided to the population. In this scenario, structural designs must be developed to decrease the damage induced by these actions. The objective of this work is to design a hybrid controller based on the H∞ optimization via state feedback and the magneto-rheological damper (MRD) to mitigate the excessive vibrations of a three-story steel frame building, represented through the shear building model, subjected to the simultaneous dynamic action of wind and earthquake. All research is based on computational simulation; experimental research and results will not be addressed. In the numerical analysis, digital computers and MATLAB® software are used, and implemented codes generate the expected results based on the mathematical modeling. With the application of the H∞ control technique via state feedback, the displacements were reduced by 77%. With MRD, this reduction was 79%. With the hybrid controller, this reduction was 100%. Thus, the verifications in relation to maximum displacements were met for NBR 15421:2006, NBR 8800:2008, and NBR 6118:2014. From the results, it can be concluded that the hybrid controller proved to be more efficient and achieved the proposed objective. The exogenous inputs had zero influence on the behavior of the system output.

Keywords: shear building; earthquake; wind; H∞ control; MRD; hybrid controller

1. Introduction

Nowadays, natural disasters are increasingly present in humanity's daily lives. They have had increasingly intense frequency and consequences. They cause economic, social, and environmental impacts. That is why it is becoming increasingly important to know about their occurrence, mechanisms, prevention measures, and damage mitigation. These disasters can be caused by various phenomena, such as earthquakes, tornadoes, hurricanes, and storms, among others [1].

The dynamic loads from earthquakes and winds can destroy lives, cause a collapse in civil structures, and interrupt basic services provided to the population. In this scenario, structural designs must be developed to reduce the damage induced by these actions. It is becoming increasingly necessary to have a correct and real representation of both the structural behavior and the wind and earthquakes to ensure structural safety [2].

With the increase in population and the verticalization of cities, structures have become more subject to vibrations due to tall, slim, flexible, and lightweight structural designs. Although the structure can suffer displacements without collapse, excessive

vibrations become a problem when the service situations of the building are verified. The low damping of high-strength materials and the use of precast structures, in which the connections are fully hinged or partially clamped, can justify this behavior [3].

Thus, searching for techniques that mitigate the effects of these actions on structures is of real importance because they can ensure the life of the building and the safety of people. Therefore, it is increasingly necessary to study these natural phenomena for their correct understanding and representation in order to analyze their behavior in real structures. Thus, interest in investigating and developing control techniques that improve the dynamic behavior of structures has increased [4].

The parameters of mass, stiffness, and damping govern the dynamic behavior of a structure. Therefore, the simplest way for a structure to behave satisfactorily with vibrations is to ensure its flexibility to absorb part of the excitation while remaining firm enough to resist the other loads. However, these techniques may be unsatisfactory to ensure structural stability under excessive vibrations, especially when they present frequencies close to the natural frequencies of the structure, which can cause resonance and consequently structural collapse [5].

The control of the amplitude of the vibrations of structures proves to be fundamental, especially in cases of resonance [6–8]. In several cases, just increasing the stiffness and mass of the system does not solve the problem since the natural frequencies are modified. Structural control is a technology for protecting structures that promotes a change in the stiffness and damping properties of the structure. To do this, external devices are added, which reduce the effects of the induced excitation by changing the dynamic characteristics of the structure. This way, the vibration energy is transformed into dissipation energy, reducing the level of damage suffered by the main structure. These control devices can be classified as passive, active, hybrid, or semi-active. They aim to reduce structural displacements by improving their behavior in service [9].

Structural vibration control has increased significantly in recent decades. One of the application areas for control design is the protection of civil engineering structures from dynamic loading, such as wind and strong earthquakes. In this context, the objective of this work is to design a hybrid controller based on H∞ optimization via state feedback and the magneto-rheological damper (MRD) to mitigate excessive vibrations caused by the dynamic action of wind and earthquake in a three-story metal frame building, represented through the shear building model. All research is based on computational simulation; tests and experimental results will not be addressed.

2. Mathematical formulation

2.1. Balance equations

The shear building model is used to model a three-story building, as illustrated in **Figure 1**.

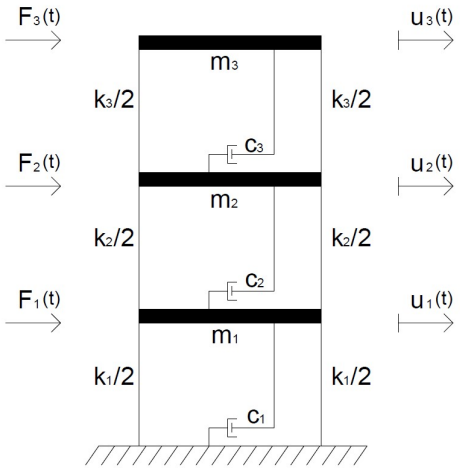

Figure 1. Shear building model with three stories.

where: mass, stiffness and damping of each floor type; $u_i(t)$: displacement as a function of time on each floor type; $F_i(t)$: external force as a function of time on each floor type; where: $i = 1, 2$ and 3, that corresponds to the number of floors.

The building is symmetric, the slabs are infinitely rigid, and the columns do not undergo axial deformation. And consequently, the only motion of the nodes is horizontal. You have three masses concentrated at the level of the floors, connected by bars that have stiffness and dampen the columns of that floor [10,11].

The equations of motion of each floor can be determined by the Euler-Lagrange method in terms of the kinetic and potential energy of the body [12]. As such, Equation (1) represents the system of equilibrium equations for the model studied:

$$\begin{cases} m_1\ddot{u}_1 + (c_1 + c_2)\dot{u}_1 - c_2\dot{u}_2 + (k_1 + k_2)u_1 - k_2u_2 = F_1(t) \\ m_2\ddot{u}_2 + (c_2 + c_3)\dot{u}_2 - c_2\dot{u}_1 - c_3\dot{u}_3 + (k_2 + k_3)u_2 - k_2u_1 - k_3u_3 = F_2(t) \\ m_3\ddot{u}_3 - c_3\dot{u}_2 + c_3\dot{u}_3 - k_3u_2 + k_3u_3 = F_3(t) \end{cases} \quad (1)$$

To facilitate analysis, it is possible to transform the system of Equations (1) into a system of first-order ordinary differential equations. Thus, let:

$$u_1 = y_1; \dot{y}_1 = y_2; u_2 = y_3; \dot{y}_3 = y_4; u_3 = y_5; \dot{y}_5 = y_6 \quad (2)$$

Deriving Equation (2) with respect to time, we have the following relations:

$$\begin{gathered} \dot{u}_1 = \dot{y}_1 = y_2; \ddot{y}_1 = \dot{y}_2 = \ddot{u}_1; \dot{u}_2 = \dot{y}_3 = y_4; \\ \ddot{y}_3 = \dot{y}_4 = \ddot{u}_2; \dot{u}_3 = \dot{y}_5 = y_6; \ddot{y}_5 = \dot{y}_6 = \ddot{u}_3. \end{gathered} \quad (3)$$

Substituting the definitions made in Equations (2) and (3) in the system of Equation (1), isolating the first-order derivatives in each of the equations, considering that there is no external excitation, and adding the new variables to the system, we have:

$$\begin{cases} \dot{y}_1 = y_2 \\ \dot{y}_2 = -\dfrac{(k_1 + k_2)y_1}{m_1} - \dfrac{(c_1 + c_2)y_2}{m_1} + \dfrac{k_2y_3}{m_1} + \dfrac{c_2y_4}{m_1} \\ \dot{y}_3 = y_4 \\ \dot{y}_4 = \dfrac{k_2y_1}{m_2} + \dfrac{c_2y_2}{m_2} - \dfrac{(k_2 + k_3)y_3}{m_2} - \dfrac{(c_2 + c_3)y_4}{m_2} + \dfrac{k_3y_5}{m_2} + \dfrac{c_3y_6}{m_2} \\ \dot{y}_5 = y_6 \\ \dot{y}_6 = \dfrac{k_3y_3}{m_3} + \dfrac{c_3y_4}{m_3} - \dfrac{k_3y_5}{m_3} - \dfrac{c_3y_6}{m_3} \end{cases} \quad (4)$$

Thus, the Jacobian matrix of the system linearized by Taylor series around the equilibrium point is:

$$J = \begin{bmatrix} 0 & 1 & 0 & 0 & 0 & 0 \\ \frac{-(k_1+k_2)}{m_1} & \frac{-(c_1+c_2)}{m_1} & \frac{k_2}{m_1} & \frac{c_2}{m_1} & 0 & 0 \\ 0 & 0 & 0 & 1 & 0 & 0 \\ \frac{k_2}{m_2} & \frac{c_2}{m_2} & \frac{-(k_2+k_3)}{m_2} & \frac{-(c_2+c_3)}{m_2} & \frac{k_3}{m_2} & \frac{c_3}{m_2} \\ 0 & 0 & 0 & 0 & 0 & 0 \\ 0 & 0 & \frac{k_3}{m_3} & \frac{c_3}{m_3} & -\frac{k_3}{m_3} & -\frac{c_3}{m_3} \end{bmatrix} \quad (5)$$

For the numerical simulations, the physical parameters presented in **Table 1** were adopted, which were used by Chopra [13] and Corbani [14]. This example deals with a steel-frame building, and the damping of the structure is represented by the Rayleigh damping matrix, with a damping rate in the first two vibration modes of 5%.

The modulus of elasticity *E* of 205 GPa was used, the height of the columns l_i on all floors is 3 m, and the yield strength f_y is 250 MPa (steel A36).

Table 1. Physical parameters of the model.

Floor	Mass (Kg)	Stiffness (N/m)
1	45,344	33,379,175
2	45,344	25,603,543
3	45,344	15,250,045

With the definitions of the physical characteristics of the structure, the natural frequencies can be obtained, which are indicated in Equation (6). To determine the system's eigenfrequencies, a motion analysis is performed in a free vibration regime without damping.

$$\omega = \begin{bmatrix} 10.80 \\ 26.33 \\ 41.57 \end{bmatrix} (\text{rad/s}) \quad (6)$$

For the dynamic wind actions of the model studied, this will be the external force caused by the wind. For this, NBR 6123 [15] will be used, which establishes parameters and definitions to determine the forces due to wind in buildings. The modified synthetic wind method proposed by Carril [16] will also be used. For calculation purposes, the wind will be considered a time-series load obtained through the Davenport spectrum. The necessary data regarding the structure characteristics and wind parameters defined by NBR 6123 [15] are listed in **Table 2**.

The series of loads that generate the load histories is obtained by summing the harmonic components according to a pseudo-random determination of the phase angles, thus giving a random representation to the process [17]:

$$q(t) = \sum_{k=1}^{m} cc_k \cos(\omega_k t - \theta_k) \quad (7)$$

As the davenport spectrum is used (**Figure 2**), the method suggests that the frequency range of 0.0017 Hz to 2.5 Hz is chosen for the decomposition of the power spectrum, i.e., periods from 0.4 s to 600 s. The fluctuating portion of the wind pressure $q(t)$ can be represented by at least 11 harmonics, one of them being the resonant, and the others multiples or submultiples of this choice, using the factor 2 [16].

Table 2. Properties of the building geometry and wind characteristics.

Parameters	**Value**
$\boldsymbol{h}$	9 m
Building dimension	28.30 m × 12.20 m
$\boldsymbol{V_0}$	45 m/s
Building category	IV
Land class	B
$\boldsymbol{S_1}$	1
$\boldsymbol{S_3}$	1.1
$\boldsymbol{C_a}$	1.2
$\boldsymbol{b}$	0.85
$\boldsymbol{p}$	0.125
$\boldsymbol{\xi}$	1.5

where: h: height of the building; V_0: basic wind speed; S_1: topographic factor; S_2: statistical factor; C_a: drag coefficient; b: the parameter as a function of the terrain category; p the exponent of the potential law of variation of S_2; ξ: dynamic amplification coefficient.

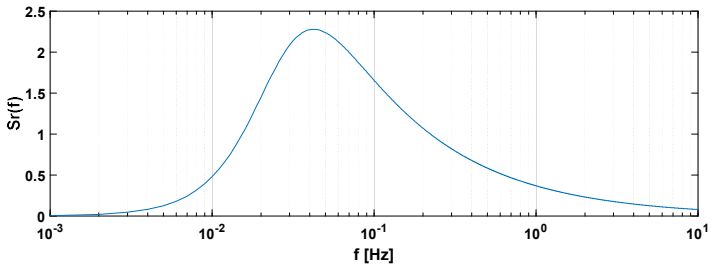

Figure 2. Wind power spectrum (davenport).

The choice of the phase angles (θ_k) of each of the 11 harmonics is obtained randomly, between $0 \leq \theta_k \leq 2\pi$, for each θ_k a loading pressure in time will be defined. The statistical analysis is done using the Monte Carlo technique [17], randomly generating 20 loading histories for the structure. Taking into account the Gaussian distribution, the displacement with a 95% probability of occurrence, which limits to only 5% the probability of this value being exceeded, is the characteristic displacement. The time series whose response is closest to the statistically determined characteristic response is adopted. According to Carril [16], this is a good representation of the characteristics of the real wind.

For the dynamic actions of the earthquake in the model studied, $F_1(t)$ will be the external force caused by the earthquake. For this, NBR 15421 [18] will be used, which establishes parameters and criteria to determine the earthquake forces on structures.

The methodology used will be based on the synthetic wind model, addressed in the works of Corbani [14] and Brandão [19]. For calculation purposes, the earthquake will be considered a time series loading, obtained through the Kanai-Tajimi spectrum [20]. The necessary data regarding the characteristics of the structure, the soil, and the earthquake parameters defined by NBR 15421 [18] are listed in **Table 3**.

With the aid of MATLAB® [21], the power spectral density function (PSDF) was generated. To obtain the values of the frequencies of the harmonic components, the suggestion of Corbani [14] was adopted: use multiples and submultiples with a factor equal to the ratio between the natural frequencies of the first and second vibration modes, being $\Delta\omega = 0.41$. **Figure 3** represents the Kanai-Tajimi PSDF on a logarithmic scale.

In the case of earthquakes, Corbarni [14] investigated what would be the appropriate number of harmonic functions and the best position of the resonant term as a function of the natural period. Since the first natural period of the structure is $T_{n1} \cong 0.6$ s, it is obtained that the most suitable number of harmonic functions to represent the earthquake are 11 harmonics, with the seventh resonant term.

Table 3. Structure, soil and earthquake parameters.

Parameters	**Value**
Zone	4
$\boldsymbol{a_g}$	0.15 g
Seismic category	C
Land class	B
Land type	Rock
$\boldsymbol{I}$	1.5
$\boldsymbol{R}$	3.5
$\boldsymbol{H}$	0.6
$\boldsymbol{\omega_g}$	27 rad/s

where a_g: horizontal seismic accelerations; $g = 9.81$ m/s^2 (acceleration of gravity); I: importance of use factor; R: response coefficient; H: damping of the soil; ω_g: characteristic natural frequency of the land.

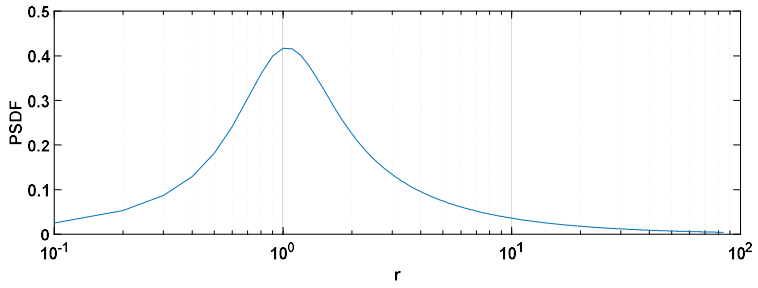

Figure 3. Kanai-Tajimi PSDF.

Aiming to determine the maximum earthquake acceleration ($\ddot{u}_g$), adapting Equation (7), and using the parameters of NBR 15421 [18], the harmonic combination of accelerations will be given by the expression:

$$\ddot{u}_g(t) = \frac{I}{R} a_g \sum_{k=1}^{m} C_k \cos(\omega_k t - \theta_k) \tag{8}$$

Analogously to the methodology of the statistical analysis for wind action, the values of θ_k, generated for each of the 11 harmonics corresponding to the 20 load histories will be analyzed for the determination of the characteristic loading.

Finally, the time series of the characteristic loading of the wind and earthquake is performed in order to calculate the time history of the displacements, velocities, and their phase planes. For this, the portion of the external force caused by the wind $F_3(t)$ and the earthquake $F_1(t)$ is added to Equation (4). The external force $F_2(t)$ will be considered to be zero. For seismic excitation, the dynamic loading is given by the product between the mass and the acceleration over time, in the opposite direction to this acceleration. Thus:

$$F_1(t) = -m_1 \ddot{u}_g(t) \tag{9}$$

For wind action, the harmonics of forces $F_3(t)$ and fluctuating pressures (Q), are given by:

$$F_3(t) = QAC_a\xi \tag{9}$$

$$Q = q_f q(t) \tag{10}$$

where: q_f: is the fluctuating pressure, given by the difference of the pressures obtained with the gust and average velocity, according to NBR 6123 [15].

Adding $F_1(t)$ and $F_3(t)$ in Equation (4) gives the system of equilibrium equations, considering the simultaneous action of wind and earthquake:

$$\begin{cases} \dot{y}_1 = y_2 \\ \dot{y}_2 = -\dfrac{(c_1 + c_2)y_2}{m_1} + \dfrac{c_2 y_4}{m_1} - \dfrac{(k_1 + k_2)y_1}{m_1} + \dfrac{k_2 y_3}{m_1} - \ddot{u}_g(t) \\ \dot{y}_3 = y_4 \\ \dot{y}_4 = -\dfrac{(c_2 + c_3)y_4}{m_2} + \dfrac{c_2 y_2}{m_2} + \dfrac{c_3 y_6}{m_2} - \dfrac{(k_2 + k_3)y_3}{m_2} + \dfrac{k_2 y_1}{m_2} + \dfrac{k_3 y_5}{m_2} \\ \dot{y}_5 = y_6 \\ \dot{y}_6 = \dfrac{c_3 y_4}{m_3} - \dfrac{c_3 y_6}{m_3} + \dfrac{k_3 y_3}{m_3} - \dfrac{k_3 y_5}{m_3} + \dfrac{F_3(t)}{m_3} \end{cases} \tag{11}$$

2.2. H∞ control via state feedback

System modeling in modern control theory can be represented by a linearized time invariant (LTI) system expressed in state space, considering the action of exogenous inputs, which represent external disturbances to the system, given by [22]:

$$\begin{aligned} \dot{x}(t) &= Ax(t) + B_2 u(t) + B_1 w(t) \\ y(t) &= Cx(t) + D_2 u(t) + D_1 w(t) \end{aligned} \tag{13}$$

where: $x(t) \in R^n$ being the state vector, $u(t) \in R^m$ the control input vector, $y(t) \in R^q$ the system outputs, $A \in R^{n \times n}$ the dynamic matrix, $B_2 \in R^{nxm}$ the control input matrix, $B_1 \in R^{nxm}$ the disturbance input matrix, $w(t) \in R^m$ the disturbance vector, $C \in R^{q \times n}$ the output matrix, $D_2 \in R^{q \times m}$ the control direct transmission matrix, and $D_1 \in R^{q \times m}$ the disturbance direct transmission matrix.

The goal is to find a matrix $K \in R^{mxn}$, called the feedback gain matrix or control matrix [23], that satisfies the condition:

$$u(t) = Kx(t) \tag{14}$$

Substituting Equation (14) into Equation (13) makes the system closed loop, that is, the system controlled with state feedback:

$$\begin{aligned} \dot{x}(t) &= (A + B_2K)x(t) + B_1w(t) \\ y(t) &= (C + D_2K)x(t) + D_1w(t) \end{aligned} \tag{15}$$

Since Equation (15) is linear, its stability will be defined by the eigenvalues of the matrix $A_n = (A + B_2K)$. Thus, for a controllable and asymptotically stable system, the feedback gain K can be chosen such that all eigenvalues of A_n have the negative real part.

For the correct formulation of the problem, it is first necessary to define the norm H∞. Considering the Equation (13) with $u(t) = 0$, then its norm H∞ is characterized by the largest value of the modulus of the relationship between the frequency of the output signals $y(t)$ and the exogenous input $w(t)$ [24]. It is mathematically defined by:

$$\|H(s)\|_\infty = \max_{\omega \in \mathbb{R}^+} \sigma_{\max}(H(j\omega)) = \max_{\omega \in \mathbb{R}^+} \frac{|Y(j\omega)|}{|W(j\omega)|} \tag{16}$$

where: $H(s)$ is the transfer function relating the output $y(t)$ and the exogenous input $w(t)$ of the system (15), $Y(j\omega)$ is the frequency response of the output $y(t)$ and $W(j\omega)$ is the frequency response of the exogenous input $w(t)$.

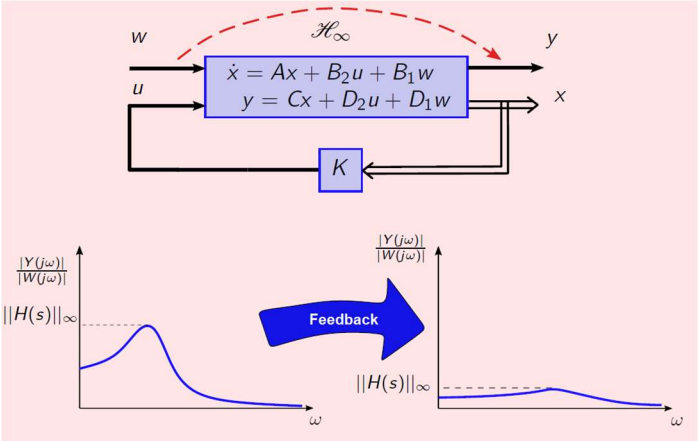

Figure 4. Optimal control H∞.

The goal is to design a controller $K \in R^{mxn}$, such that $u(t) = Kx(t)$, that asymptotically stabilizes and minimizes the impacts of the exogenous input $w(t)$ on the output $y(t)$ by "sinking" the H∞ norm of the closed-loop Equation (15) through state feedback. This idea, which is called optimal control H∞, is represented in **Figure 4**. The graph in **Figure 4** is known as the Bode diagram. The H norm of the system is characterized by the largest value of the modulus of the $Y(j\omega)/W(j\omega)$, ratio, that is, the largest value of the frequency response $|H(j\omega)|$. Thus, the H∞ norm is associated with the worst case, the maximum value of $|H(j\omega)|$ indicates the case of the greatest impact that the exogenous input $w(t)$ causes on the output of the system $y(t)$.

The Equation (15) is stabilized by state feedback if, and only if, there exists a solution to the convex optimization problem [25]:

$$\min\mu$$

subject to

$$W = W' > 0$$
$$\begin{bmatrix} AW + WA' + B_2Z + Z'B_2{}' & WC' + Z'D_2{}' & B_1 \\ CW + D_2Z & -\mu I & D_1 \\ B_1{}' & D_1{}' & -I \end{bmatrix} < 0 \quad (17)$$

In the optimal solution, $K = ZW^{-1}$ ensures $\|H(s)\|_\infty \leq \sqrt{\mu}$. Further details can be found in the study of Boyd et al. [25]. The proof of LMI Equation (17) can be found in the works by Palma and Peres [26,27].

Since the dynamic equations of Equation (12) are linear and time-invariant equations, the shear building model with three floors can be rewritten in the state space form of Equation (13). In the structural model of the building, **Figure 1**, the control force $F_c(t)$, acting on the 3rd floor will be considered, which will be seen as the actuator of the controllers. It was defined that the input vector $u(t) = F_c(t)$, will be given by Equation (14). The exogenous inputs $w(t)$ will be provided by the wind and earthquake action. The state vector $x(t)$ and the output vector $y(t)$ will be composed of six elements, according to the system of Equation (12):

$$x(t) = \begin{bmatrix} y_1 \\ y_2 \\ y_3 \\ y_4 \\ y_5 \\ y_6 \end{bmatrix}, y(t) = \begin{bmatrix} y_1 \\ y_2 \\ y_3 \\ y_4 \\ y_5 \\ y_6 \end{bmatrix} \quad (18)$$

Thus, from the system of dynamic Equation (12) and the vectors $u(t)$, $x(t)$, $y(t)$ defined in Equations (14) and (18), respectively, the matrices in Equation (13), which correspond to the representation of the shear building model in state space form, will be given by:

$$A = \begin{bmatrix} 0 & 1 & 0 & 0 & 0 & 0 \\ \frac{-(k_1+k_2)}{m_1} & \frac{-(c_1+c_2)}{m_1} & \frac{k_2}{m_1} & \frac{c_2}{m_1} & 0 & 0 \\ 0 & 0 & 0 & 1 & 0 & 0 \\ \frac{k_2}{m_2} & \frac{c_2}{m_2} & \frac{-(k_2+k_3)}{m_2} & \frac{-(c_2+c_3)}{m_2} & \frac{k_3}{m_2} & \frac{c_3}{m_2} \\ 0 & 0 & 0 & 0 & 0 & 0 \\ 0 & 0 & \frac{k_3}{m_3} & \frac{c_3}{m_3} & -\frac{k_3}{m_3} & -\frac{c_3}{m_3} \end{bmatrix} \quad (19)$$

$$B_2 = \begin{bmatrix} 0 \\ 0 \\ 0 \\ 0 \\ 0 \\ 1/m_3 \end{bmatrix}, C = \begin{bmatrix} 1 & 0 & 0 & 0 & 0 & 0 \\ 0 & 1 & 0 & 0 & 0 & 0 \\ 0 & 0 & 1 & 0 & 0 & 0 \\ 0 & 0 & 0 & 1 & 0 & 0 \\ 0 & 0 & 0 & 0 & 1 & 0 \\ 0 & 0 & 0 & 0 & 0 & 1 \end{bmatrix}, D_2 = D_1 = 0 \quad (20)$$

$$B_{1(v+s)} = \begin{bmatrix} 0 & 0 \\ 0 & -1 \\ 0 & 0 \\ 0 & 0 \\ 0 & 0 \\ 1/m_3 & 0 \end{bmatrix}, w_{(v+s)}(t) = \begin{bmatrix} F_3(t) \\ \ddot{u}_g(t) \end{bmatrix} \quad (21)$$

where: $B_{1(v+s)}$ e $w_{(v+s)}(t)$ refers to the simultaneous exogenous input of wind and earthquake.

By grouping these matrices according to Equation (13), the complete representation of the model studied in the form of state space can be obtained. Using the Sedumi solver of MATLAB® [21], the controller H∞ was obtained by solving the LMI in Equation (17) [28].

2.3. MRD

MRD are semi-active control devices that can have their damping factor changed instantaneously, have high stability, reliability, and operate silently. Considered an intelligent material, the magneto-rheological (MR) fluid is a mixture of oil with ferromagnetic micro-particles that are sensitive to the action of a magnetic field. And when it is exposed to a magnetic field strength or electric current, it changes from a free-flowing liquid into a semisolid with controllable force strength. The ferromagnetic particles tend to align themselves into linear structures, parallel to the magnetic flow lines, which hinder the flow of the fluid and consequently increase its viscosity [7].

For the development of the control system of MR actuators, it is necessary that the mathematical model be faithful to their dynamic behavior. The most referenced and used in most research involving MRD is the modified Bouc-Wen parametric model, presented in the work of Spencer [29], **Figure 5**. It arose from the Bouc-Wen model, which depicts the behavior of a typical MRD.

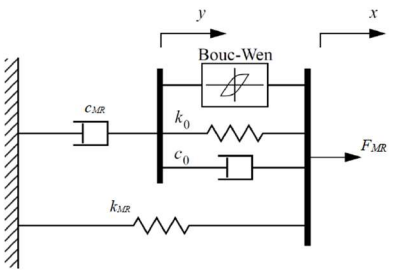

Figure 5. Modified Bouc-Wen model.

The equations governing the dynamic behavior of the modified Bouc-Wen model are described by [7,29]:

$$c_{MR}\dot{y} = \alpha z + k_0(x - y) + c_0(\dot{x} - \dot{y}) \quad (22)$$

The variable z can be obtained by the equation:

$$\dot{z} = -\gamma|\dot{x} - \dot{y}|z|z|^{n-1} - \beta(\dot{x} - \dot{y})|z|^n + A(\dot{x} - \dot{y}) \quad (23)$$

Solving Equation (22) as a function of $\dot{y}$, we get:

$$\dot{y} = \frac{1}{c_0 + c_{MR}}[\alpha z + + c_0\dot{x} + k_0(x - y)] \tag{24}$$

The total strength of the modified Bouc-Wen model is given by:

$$F_{MR} = \alpha z + k_0(x - y) + c_0(\dot{x} - \dot{y}) + k_{MR}(x - x_0) \tag{25}$$

It can be rewritten as follows:

$$F_{MR} = c_{MR}\dot{y} + k_{MR}(x - x_0) \tag{26}$$

where: F_{MR} is the force generated by the MRD; c_{MR} is the damping factor of the MRD; k_{MR} is the stiffness associated with the MRD; $\dot{y}$ is the velocity of the MRD's piston embolus; x is the displacement of the MRD; c_0 is the initial damping factor; k_0 is the initial stiffness coefficient of the assembly; x_0 is the initial displacement of the MRD; γ, β, n and A, depend on the characteristics of the damper.

In this methodology, many parameters are required to characterize the MRD. Their optimized values are determined by fitting the prototype according to experimental data obtained in laboratory tests. This model is the one that presents the highest accuracy, however, when used in control systems, the solution of all these equations naturally requires a certain computational effort, since it has three differential equations, besides the equations of the electric circuit dynamics [7,29].

In order to circumvent this problem, this paper proposes to use an approximate expression for Equation (26). Where force F_{MR} does not explicitly present a dependence on the control variable, which should be the electric current. According to Tusset and Balthazar [30], who conducted studies on MRD behavior and used experimental data to write the function Equation (27) that is dependent on the electric current:

$$F_{MR} = \frac{3.2}{(3e^{-3.4i}) + 1}\dot{x} + k_0 x + \frac{8.5}{(1.28e^{-3.9i}) + 1}z \tag{27}$$

2.4. H∞ hybrid controller and MRD

In order to further reduce the amplitudes of the temporal responses, it is proposed in this paper to use hybrid control, which is a combination of active control and semi-active control. The H∞ controller via state feedback will be the active control, and the MRD controller will be the semi-active control. **Figure 6** shows the structural model of the building, considering the hybrid controller.

Putting the two controls together from Equation (15), we have:

$$\begin{gathered} \dot{x}(t) = (A + B_2K)x(t) + B_1w(t) + B_3f(t) \\ y(t) = (C + D_2K)x(t) + D_1w(t) \end{gathered} \tag{28}$$

where: $f(t)$ is the MRB force vector and B_3 is the MRB input matrix.

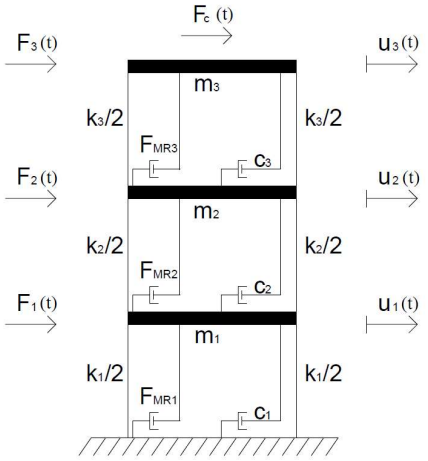

Figure 6. Shear building model with action of the controlled hybrid.

To solve Equation (28), the theories discussed in sections 2.2 and 2.4 will be adopted. The components of Equation (28), corresponding to MRB, are:

$$B_3 = \begin{bmatrix} 0 & 0 & 0 \\ -1/m_1 & 1/m_1 & 0 \\ 0 & 0 & 0 \\ 0 & -1/m_2 & 1/m_2 \\ 0 & 0 & 0 \\ 0 & 0 & -1/m_3 \end{bmatrix}, f(t) = \begin{bmatrix} F_{MR1} \\ F_{MR} \\ F_{MR3} \end{bmatrix} \tag{29}$$

3. Results and discussion

Initially, the stability of the structure was analyzed for the nominal physical parameters (**Table 1**), null initial conditions, and no external force. The eigenvalues of the Jacobian matrix were computationally calculated in Equation (5), which classified the structure as stable, according to Lyapunov [31]. Thus, it can be verified that the model studied is naturally stable.

In order to analyze the robustness of the structural stability, the verification was repeated, considering a 10% uncertainty for the stiffness values and keeping the other values in **Table 1** fixed. For all combinations, the structure presents stable behavior. For a civil structure, which is the case of the model studied, the stability points are related to the non-occurrence of the following structural conditions: loss of equilibrium, exhaustion of resistant capacity, or collapse.

For the temporal responses to wind and earthquake action, null initial conditions will be considered for displacements and velocities, the physical parameters presented in **Tables 1–3**. This requires the integration over time of the system of first-order ordinary differential equations by some numerical method. In this work, the chosen technique is the 4th-order Runge-Kutta method [12], which presents good numerical stability.

The results of the numerical simulations consider the simultaneous action of wind and earthquake. The response is analyzed for 50 s with a step of 0.01, which corresponds to 5000 points. This amount of points is necessary to observe transient

behavior and the permanent regime. The choice of time is based on the duration of an earthquake, as suggested by Chopra [13].

Figure 7 presents the displacement as a function of time for the joint excitation of wind and earthquake for the three floors. It can be observed that the displacements on the three floors have analogous behaviors for the same time range, which gradually increase until they stabilize and oscillate around the equilibrium point. The peaks and valleys are close together and occur with a similar frequency. The third floor presents the largest displacements, with 10.51 cm as the critical value and the displacement at the top of the building being 20.67 cm.

From the results presented for the simulations with external excitations, it can be seen that the building does not have sufficient stiffness to ensure stability against external actions. Therefore, it is necessary to calculate the Lyapunov exponent (λ) to verify if the structure presents chaotic behavior. For this, we use the algorithm developed by Mohammadi [32], which is based on the methodology of Wolf and collaborators [31] and Rosenstein and collaborators [33].

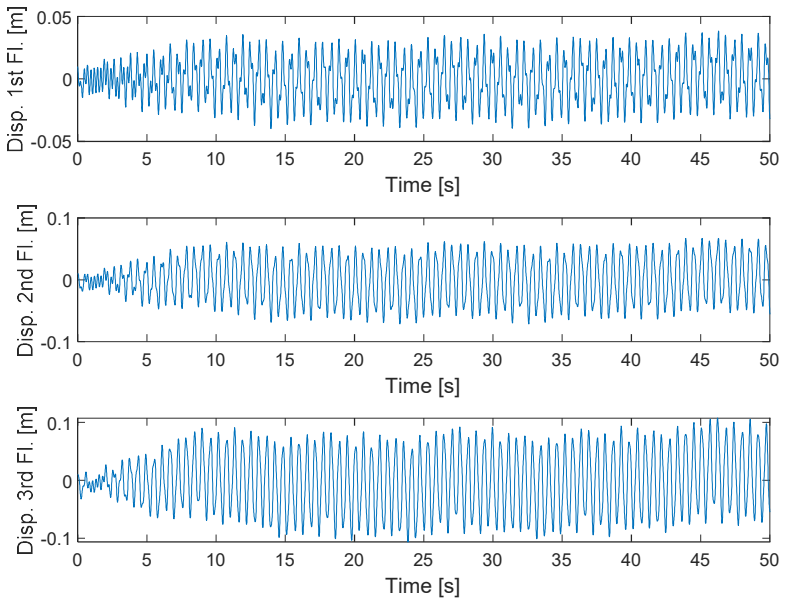

Figure 7. Temporal response with simultaneous action—displacement.

With the goal of obtaining the Lyapunov exponents, the time series obtained with the building model for the simultaneous action were cast into the algorithm. The results were: $\lambda_1 = 0.7661; \lambda_2 = 0.5114; \lambda_3 = 0.4917; \lambda_4 = 0.4903; \lambda_5 = 0.3713; \lambda_6 = 0.396$.

The model has six dimensions, so it has six Lyapunov exponents. They were ordered from highest to lowest [8]. It can be observed that the values of the Lyapunov exponents showed variations, which means that the divergence rate of the trajectories was expressive. It can be concluded that all Lyapunov exponents are positive, meaning that the system is hyperchaotic. According to Savi [12], this implies that the trajectory diverges exponentially from the original orbit, indicating a non-stable system of the chaotic type, which characterizes the total or partial collapse of the structure. Because the structure no longer presents stable behavior but chaotic behavior, it is necessary to apply control techniques that allow structural integrity under the effect of the presented

excitations.

Applying the H∞ control technique via state feedback to the system studied the following feedback gain was obtained:

$$K = [-2.3113 \quad 0.1516 \quad 6.8743 \quad -0.0554 \quad 3.1260 \quad -0.1108] \times 10^6 \quad (30)$$

Figure 8 shows the Bode diagram for the system with control (red color) and the system without control (blue color). It can be observed that there was a "sinking" of the H∞ standard, after the control by state feedback. With this, the exogenous input of the simultaneous action $w_{(v+s)}(t)$ will have minimal influence on the behavior of the system output $y(t)$. And this behavior can be observed in **Figure 9**, which compares the temporal responses of the displacements of the system with control and without control. It can be seen that the amplitudes were reduced considerably in the controlled system.

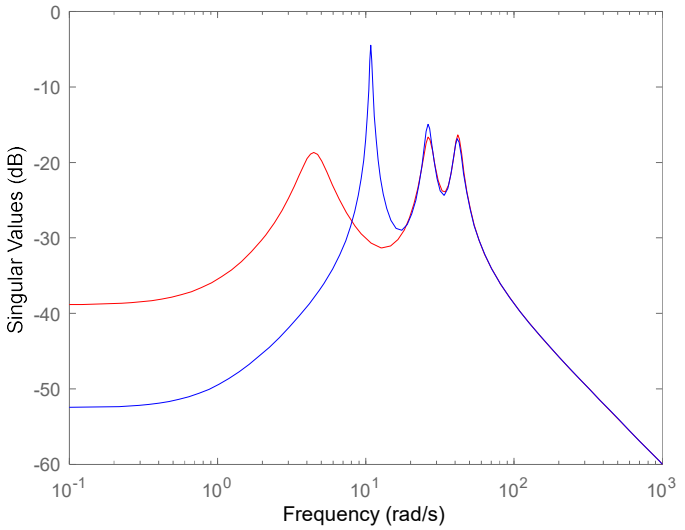

Figure 8. Bode diagram—simultaneous action.

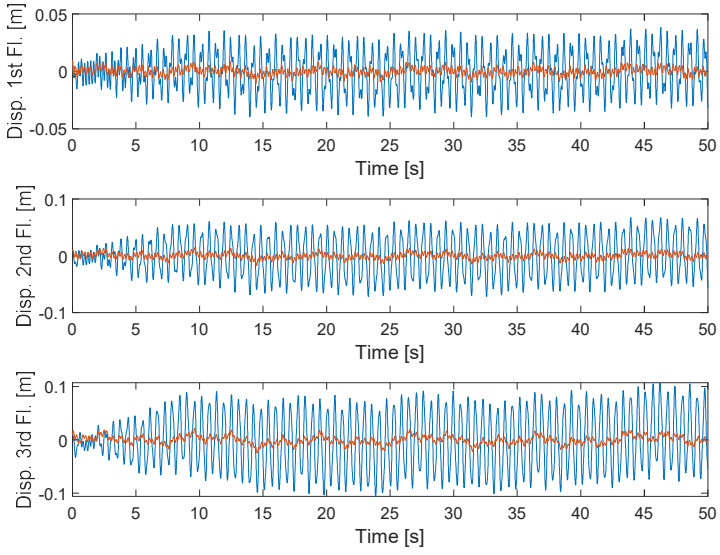

Figure 9. H∞ control for simultaneous action—displacement.

When evaluating seismic performance, one must verify whether the structural displacements may imply damage or a loss of stability. The limit displacements, in

relation to the floors established by the standard, apply to seismic categories B or C and depend on the type of occupancy of the building as established in NBR 15421 [18], being limited to $h/100$. NBR 8800 [34] recommends a relationship of $H/400$ for displacements at the top of the building and $h/500$ between floors, where H is the total height of the building and h is the height of the ceiling. NBR 6118 [35] recommends that for non-structural elements, such as walls, the lateral displacement of buildings should be a maximum of $H/1700$ for the top and $h/850$ between floors. This large difference between the criteria is justified by the fact that non-structural elements have low strength and modulus of elasticity. Therefore, a stricter displacement criterion is necessary to avoid collapse.

Table 4 shows the comparative maximum displacements of the system in open loop (OL) and closed loop (CL). For the total displacement, the maximum displacements on the three floors were added, and in the relationship between the floors, the 3rd floor was adopted because it is the most critical. The total height of the building studied is 9 m, and the height of the typical floor is 3 m. After the H∞ control via state feedback, the total displacement of the structure presented a reduction of 77%, while the maximum displacement of the 3rd floor presented a reduction of 79%. Despite the significant reduction, the values were still above the limit determined by NBR 8800 [34] and NBR 6118 [35]. When analyzing NBR 15421 [18], the reduction in displacement was enough to leave it below the limit.

Table 4. Maximum displacements—H∞ control for simultaneous action.

NBR	Displacement	Maximum value (cm)		Limit (cm)	Situation
		OL	CL		
8800	Top of the building	20.67	4.57	2.25	Above
	Between floors	10.51	2.15	0.60	Above
6118	Top of the building	20.67	4.57	0.53	Above
	Between floors	10.51	2.15	0.36	Above
15421	Between floors	10.51	2.15	3.00	Below

In the application of the MRD technique, the MRD parameters used in the simulations are presented in **Table 5** [7,30]:

Table 5. MRD parameters for simulation.

Actuator parameters	Values
γ [m^{-2}]	408,720
β [m^{-2}]	−360,220
n [s^{-1}]	2
A	634
i [A]	2
k_0 [N/m]	−155.63

Implementing the functions of Section 2.3 and the parameters of **Table 5** in an

algorithm in MATLAB® [21] and integrating over time, we obtained the temporal responses shown in **Figure 10**, which compares the displacements of the system with control (red) and no control (blue). It can be seen that the amplitudes of the temporal responses were considerably reduced. When comparing **Figure 10** with **Figure 9**, it is observed that the amplitude oscillations for the MRD controller were smaller.

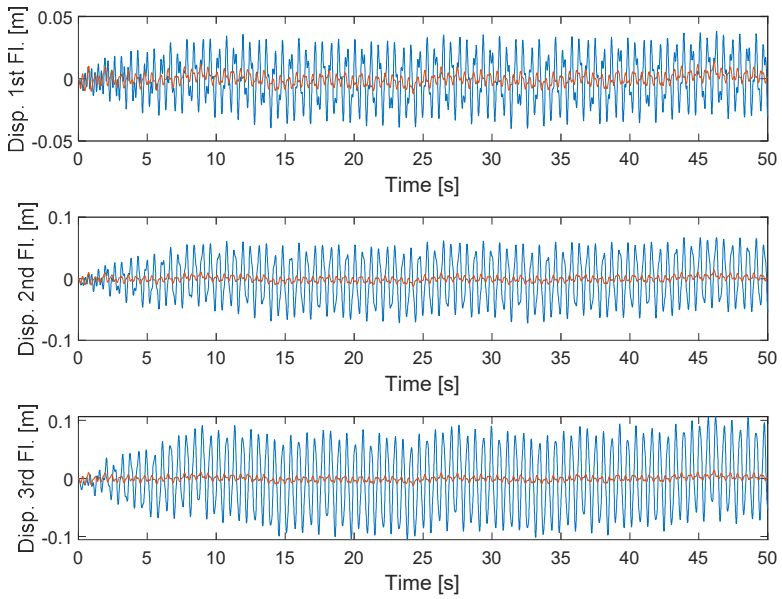

Figure 10. MRD control for simultaneous action—displacement.

Table 6 confirms this, since the displacements after the MRD control showed a total displacement of 79%, while the maximum displacement of the 3rd floor showed a reduction of 86% when compared to the values without control (OL). Analogously to the H∞ control, only the verification of NBR 15421 [18] was met.

Table 6. Maximum displacements—MRD control for simultaneous action.

NBR	Displacement	Maximum value (cm)		Limit (cm)	Situation
		OL	CL		
8800	Top of the building	20.67	4.25	2.25	Above
	Between floors	10.51	1.42	0.60	Above
6118	Top of the building	20.67	4.25	0.53	Above
	Between floors	10.51	1.42	0.36	Above
15421	Between floors	10.51	1.42	3.00	Below

In order to further reduce the amplitudes of the temporal responses, a hybrid control is used. Implementing the functions from Section 2.4 and parameters adopted in an algorithm in MATLAB® [21] and doing the integration over time, we obtained the temporal responses, illustrated in **Figure 11**. It can be observed that the temporal responses of the controlled system (red) present zero oscillations when compared to the uncontrolled system. The system remained in equilibrium over time, even with the simultaneous action of wind and earthquake.

From **Table 7**, it can be seen that the hybrid controller also presented a 100%

reduction in its maximum displacement when compared to the values without control (OL), staying below the limit established in the three analyzed standards. **Figure 12** shows the efficiency of the hybrid controller when comparing it to the H∞ and MRD, and hybrid controllers. The exogenous input $w_{(v+s)}(t)$ had zero influence on the behavior of the system output $y(t)$, thus achieving the controller's objective.

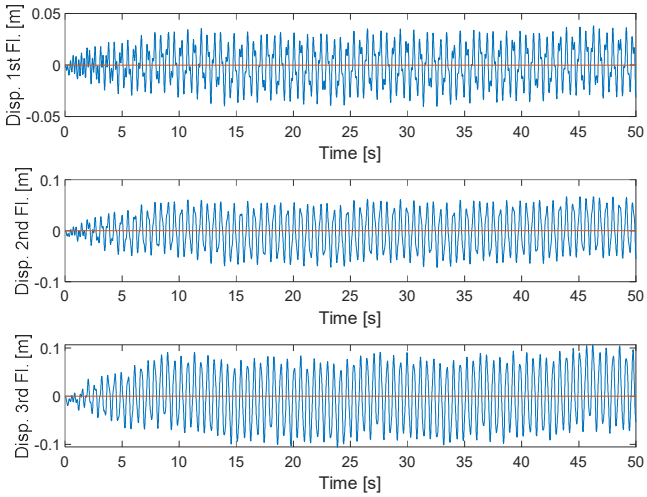

Figure 11. Hybrid control for simultaneous action—displacement.

Table 7. Maximum displacements—hybrid control for simultaneous action.

NBR	Displacement	Maximum value (cm)		Limit (cm)	Situation
		OL	CL		
8800	Top of the building	20.67	8.34×10^{-4}	2.25	Below
	Between floors	10.51	3.49×10^{-4}	0.60	Below
6118	Top of the building	20.67	8.34×10^{-4}	0.53	Below
	Between floors	10.51	3.49×10^{-4}	0.36	Below
15421	Between floors	10.51	3.49×10^{-4}	3.00	Below

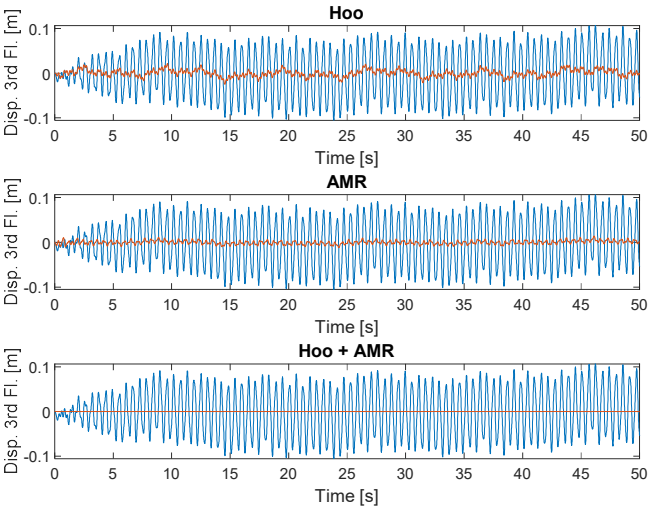

Figure 12. H∞ control, MRD and hybrid control for simultaneous action—displacement.

4. Conclusions

The natural disaster that was the focus of this work was the occurrence of seismic and wind actions in civil structures, and thus it was found that these actions increase considerably the displacements of the structure. Because the structure no longer shows stable behavior but chaotic behavior, it was necessary to apply control techniques that allow structural integrity under the effect of the presented excitations. The first control technique applied was optimization H∞ via state feedback, using the mathematical method of LMIs. With this, the system had a reduction of more than 77% in its maximum displacement. From the results presented, it can be concluded that, through state feedback and the H∞ controller design, the system was stabilized and its H∞ norm was minimized, thus achieving the controller's goal. The second control technique applied was the MRD, using the modified Bouc-Wen model. In the simulations, there was a reduction of more than 79% in the maximum displacements. With the reduction as well as the H∞ technique, only the verification of NBR 15421:2006 was met. Analyzing the presented results, it can be concluded that through the MRD controller, the system was stabilized, its oscillations were mitigated, and its displacements were reduced, thus achieving the controller's goal. Aiming to further reduce the amplitudes of the temporal responses, the hybrid control technique H∞ via state feedback and MRD was developed and applied. With this, there was a 100% reduction in their displacements. Thus, the verifications in relation to maximum displacements were met for the three standards analyzed in this work. From these results, it can be concluded that the hybrid controller proved to be more efficient and achieved the proposed objective. The exogenous inputs had no influence on the system's output behavior.

Author contributions: Conceptualization, MDdGS and FRC; methodology, MDdGS and FRC; software, MDdGS and FRC; validation, MDdGS and FRC; formal analysis, MDdGS and FRC; investigation, MDdGS and FRC; resources, MDdGS and FRC; data curation, MDdGS and FRC; writing—original draft preparation, MDdGS and FRC; writing—review and editing, MDdGS and FRC; visualization, MDdGS and FRC; supervision, MDdGS and FRC; project administration, MDdGS and FRC; funding acquisition, MDdGS and FRC. All authors have read and agreed to the published version of the manuscript.

Funding: We thank the University of Rio Verde and the Laboratory of Complex Systems (Sisplexos) in the development of the project. We thank CNPq and FAPESP for their support and encouragement of the research developed. CNPq - National Council for Scientific and Technological Development (Proc. N. 301401/2022-5). Research Support Foundation of São Paulo - FAPESP (Proc. n. 2023/00861-8).

Conflict of interest: The authors declare no conflict of interest.

References

1. Tominaga LK, Santoro J, Amaral R. Natural Disasters: Knowing to Prevent, 1st ed (Portuguese). Instituto Geológico; 2009.
2. Bosse RM. Performance of TMDs in Buildings Subjected to Earthquakes (Portuguese) [Master's thesis]. Escola de Engenharia da Universidade de São Paulo; 2017.

3. García-Illescas MA, Alvarez-Icaza L. Model reduction of shear building models: A quantitative approach for master degrees of freedom selection. Engineering Structures. 2019; 179: 512-522. doi: 10.1016/j.engstruct.2018.11.019
4. Ribeiro M. Numerical and Computational Analysis of a Wind-induced Structural Vibration Control System (Portuguese) [PhD thesis]. Universidade Federal de Juiz de Fora; 2018.
5. Pandit AR, Biswal KC. Seismic control of multi degree of freedom structure outfitted with sloped bottom tuned liquid damper. Structures. 2020; 25: 229-240. doi: 10.1016/j.istruc.2020.03.009
6. Chavarette FR, Lima RS de. Nonlinear dynamics, chaos and control of the Hindmarsh-Rose neuron model. Boletim da Sociedade Paranaense de Matemática. 2022; 40: 1-9. doi: 10.5269/bspm.47770
7. Roefero LGP, Chavarette FR, Mishra LN. Linear Quadratic Regulator Applied to a Magnetorheological Damper Aiming Attenuate Vibration in an Automotive Suspension. Twms Journal of Applied and Engineering Mathematics. 2022; 12: 1189-1201.
8. Vicente J, Chavarette F, Roefero L. Chaos Control via Mathieu-Van der Pol System and Linear Optimal Control Design with a Non-ideal Excitation and Parametric Uncertainties. Revista Internacional de Métodos Numéricos para Cálculo y Diseño en Ingeniería. 2019; 35. doi: 10.23967/j.rimni.2019.08.001
9. Bandyopadhyay S, Parulekar YM, Sengupta A, et al. Structure soil structure interaction of conventional and base-isolated building subjected to real earthquake. Structures. 2021; 32: 474-493. doi: 10.1016/j.istruc.2021.03.069
10. Brasil RMLRF, da Silva MA. Introduction to the Dynamics of Structures for Civil Engineering, 2nd ed (Portuguese). Blucher; 2015.
11. Paz M, Kim YH. Structural Dynamics. Springer International Publishing; 2019. doi: 10.1007/978-3-319-94743-3
12. Savi MA. Non-linear Dynamics and Chaos, 2nd ed (Portuguese). E-Papers; 2017.
13. Chopra AK. Dynamics of Structures: Theory and Applications to Earthquake Engineering. Prentice Hall; 1995.
14. Corbani S. Dynamic Elasto-plastic Analysis of Steel Structures Subjected to Random Earthquake Excitation (Portuguese) [Master's thesis]. Escola Politécnica da Universidade de São Paulo; 2006.
15. Associação Brasileira de Normas Técnicas. ABNT. NBR 6123. Forces Due to Wind in Buildings (Portuguese). ABNT; 1988.
16. Carril CFJ. Numerical and Experimental Analysis of the Dynamic Effect of Wind on Metal Lattice Towers for Telecommunications (Portuguese) [PhD thesis]. Escola Politécnica da Universidade de São Paulo; 2000.
17. Franco M. Direct Along Wind Dynamic Analysis of Tall Structures. Boletim Técnico; 1993.
18. Associação Brasileira de Normas Técnicas. ABNT. NBR 15421. Design of Earthquake-resistant Structures—Procedure (Portuguese). ABNT; 2006.
19. Brandão FS. Optimization of Synchronized Dynamic Attenuators for Vibration Control in Buildings Subjected to Seismic Excitation (Portuguese) [Master's thesis]. Escola de Engenharia da Universidade Federal do Rio Grande do Sul; 2021.
20. Kanai K. Semi-empirical formula for the seismic characteristics of the ground. Bulletin of the Earthquake Research Institute, University of Tokyo. 1957; 35.
21. MATLAB 2022 version. Mathworks Company.
22. Ogata K. Modern Control Engineering (Portuguese), 5th ed. Editora Pearson Prentice Hall; 2010.
23. Ferreira DC, Chavarette FR, Peruzzi NJ. Linear matrix inequalities control driven for non-ideal power source energy harvesting. Journal of Theoretical and Applied Mechanics. Published online July 23, 2015: 605. doi: 10.15632/jtam-pl.53.3.605
24. Trofino A, Coutinho DF, Barbosa KA. Improved H2 and H∞ conditions for robust analysis and control synthesis of linear systems. Sba: Controle & Automação Sociedade Brasileira de Automatica. 2005; 16(4): 427-434. doi: 10.1590/s0103-17592005000400004
25. Boyd S, El Ghaoui L, Feron E, et al. Linear Matrix Inequalities in System and Control Theory. Published online January 1994. doi: 10.1137/1.9781611970777
26. Palma PHT. Experimental Identification and Active Control of Vibrations Applied to Intelligent Structures (Portuguese) [Master's thesis]. Universidade Estadual Paulista "Júlio de Mesquita Filho"; 2007.
27. Peres PLD. H2 Control and H∞: Characterization by Linear Matrix Inequalities (Portuguese) [PhD thesis]. Universidade Estadual de Campinas; 1997.
28. Assunção E. Design of robust H2 controllers and H∞ via LMI (Portuguese). In: Class notes from the H2 and H robust controller design discipline via LMI from the electrical engineering postgraduate course at UNESP (Portuguese)—Ilha Solteira. 2019.

29. Spencer JRBF, Dyke SJ, Sain MK, Carlson JD. Phenomenological model for magnetorheological dampers. Journal of engineering mechanics. 1997; 123(3): 230-238. doi: 10.1061/(ASCE)0733-9399(1997)123:3(230)
30. Tusset AM, Balthazar JM. On the Chaotic Suppression of Both Ideal and Non-ideal Duffing Based Vibrating Systems, Using a Magnetorheological Damper. Differential Equations and Dynamical Systems. 2012; 21(1-2): 105-121. doi: 10.1007/s12591-012-0128-4
31. Wolf A, Swift JB, Swinney HL, Vastan JA. Determining Lyapunov exponents from a Time Series. Physica D. 1985; 16: 285-317. doi: 10.1016/0167-2789(85)90011-9
32. Mohammadi S. Lyaprosen: MATLAB function to calculate Lyapunov exponent. University of Tehran; 2009.
33. Rosenstein MT, Collins JJ, Deluca CJ. A practical method for calculating largest Lyapunov exponents from small data sets. Physica D. 1993; 65(1-2): 117-134. doi: 10.1016/0167-2789(93)90009-P
34. Associação Brasileira de Normas Técnicas. ABNT. NBR 8800. Design of Steel Structures and Mixed Steel and Concrete Building Structures (Portuguese). ABNT; 2008.
35. Associação Brasileira de Normas Técnicas. ABNT. NBR 6118. Design of Concrete Structures-Procedure (Portuguese). ABNT; 2014.